CHAPTER 8

8. Study of Chain Pillars Stability in Longwall Workings

8.1 General

In this chapter, the results of the numerical modelling-based parametric study to evaluate the influence of various factors on the stability of chain pillars are presented. The stability of the chain pillar was evaluated for single-row and double-row pillar layouts when both the adjoining panels were mined out. The aim of this study was to assess the variation in Factor of Safety of the chain pillar with the change in cover depth, chain pillar width, chain pillar height, abutment angle, panel width, the strength of the coal seam, moduli ratio of the roof and floor strata to the coal seam, and elastic modulus of the overburden.

The primary data of the parameters for the study were derived considering the average physico-mechanical and geo-mining properties of 27 longwall panels in different coalfields in India (Table 8.1). The average cover depth of the longwall panels varied between 49 and 865m, whereas the panel width ranged from 90 to 250m. The mining height of the workings ranged between 2.2 and 4.5m.

Table 8.1 Geo-mining details of the longwall panels

Sl. No	Coalfield	Mine	Coal seam	Panel	Average depth from surface (m)	Seam thickness/extraction height (m)	Face length (m)
1	Jharia	Moonidih	XV	T4	865.00	3.6	250
2	Jharia	Moonidih	XVIII	A4	395.45	3.56/2.55	95
3	Jharia	Moonidih	XVI Top	D13	600	2.5	150
4	Raniganj	Jhanjra	RVII	W1	56.24	3.80/3.40	120
5	Raniganj	Jhanjra	RVII	W2	49.09	4/3.70	120
6	Raniganj	Jhanjra	RVIIA	AW1	100.15	4.5/2.2	120
7	Raniganj	Jhanjra	RVIIA	AW2	97.99	2.2/4.08	120
8	Raniganj	Jhanjra	RVIIA	AE1	94.87	2.20	120

9	Raniganj	Jhanjra	RVIIA	AW3	92.80	5.2/2.2	120
10	Raniganj	Jhanjra	RVIIA	AW4	92.48	2.6/5.78	120
11	Raniganj	Jhanjra	RVIIA	AW8	112.48	4.95/2.3	120
12	Raniganj	Jhanjra	RVIIA	AW9	112	2.1/4.87	120
13	Raniganj	Jhanjra	RVI	A2E1	224.16	3.98	150
14	Raniganj	Khottadih	Samla	P1	174.05	4.5	120
15	Raniganj	Khottadih	Samla	P2	174.05	4.5	150
16	Bishrampur	Balrampur	Passang	P1	50.1	2.4	150
17	Bishrampur	Balrampur	Passang	B7	55.73	2.6/2.2	150
18	Bishrampur	New Kumda	Passang	K5	71	2.2	150
19	Sohagpur	Rajendra	Burhar VIB	P2	74	3.0/2.2	150
20	Sonhat	Churcha	V	P1	218.29	3.2/3.0	150
21	Godavari Valley	PVK	I	21	212.30	3.0	150
22	Godavari Valley	VK7	I	4	187.88	11.42/2.70	150
23	Godavari Valley	JK5	Queen	3	194.32	15.68/3	135
24	Godavari Valley	GDK 9	3	3T	127	3	150
25	Godavari Valley	GDK10A	I	11	255.50	6-6.5/3	112
26	Godavari Valley	GDK10A	I	12	288.7	6/3	102
27	Godavari Valley	Adriyala	I	P1	450	3.5	250

The formulation and solution scheme of the numerical model used for this purpose is described in Section 3.8, Chapter 3. The coal seam was assigned an elastic constitutive model to determine the Factor of Safety of the pillar under different conditions.

In the basic numerical model, the extent of the caving zone comprising the immediate roof and the main roof was 15 times the extraction height, as described in Chapter 6. The extent of the Fractured zone was considered 28 times the extraction height. In contrast, the truncated overburden strata up to 150 m from the Fractured zone were considered the Continuous Deformation zone. The vertical stress equivalent to the remaining thickness of the overburden was initialized at the model top. The thickness of floor strata was taken as 200 m to satisfy the infinite elastic boundary conditions in deep mine workings.

The abutment angle for a given geo-mining condition was estimated by the statistical model (Equation 7.3) developed in Chapter 7. The rock mass parameters for the Caved, Fractured and Continuous Deformation zones were determined using the approach developed in Chapter 6.

The parametric study was designed keeping in mind the prevailing and future scenario of longwall workings in the Indian conditions. Figures 8.1 (i)-(x) illustrate the range of the parameters considered in the study. The cover depth varies from 350 to 900m. The Regulation

111 of Coal Mines Regulation, 2017 (DGMS, 2017) stipulates pillar size up to the maximum depth of 360m. No specific guideline is available for the selection of the pillar size beyond this depth. The cover depth of 900m corresponds to the maximum depth of the longwall to be mined in the near future in Indian conditions. The pillar size varied from 25 to 100m for single-row chain pillars, while it varied from 10 to 47.5 m for the double row configuration. The variation in face length was done from 150 to 250m considering feasible face length at such depth and currently prevailing practices in the Indian conditions. Similarly, pillar height varied between 2.5 to 4.5m. The roof strata and coal seam were categorized into soft, medium, and hard depending on their compressive and tensile strength.

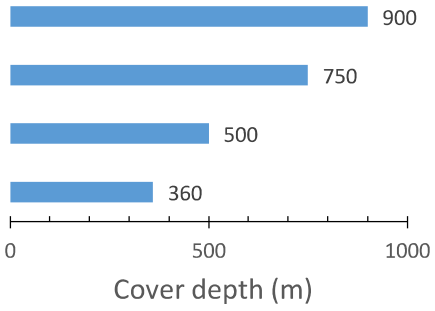

(i)

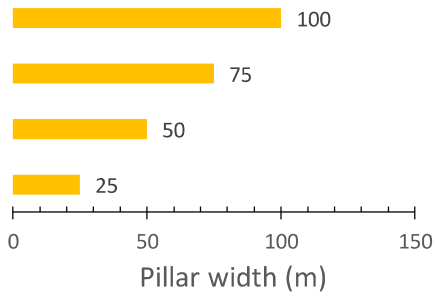

(ii)

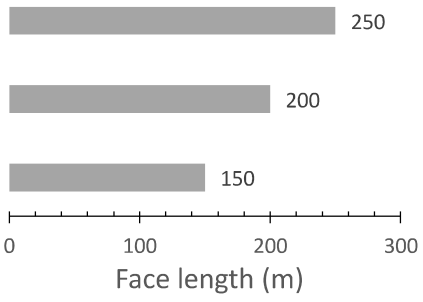

(iii)

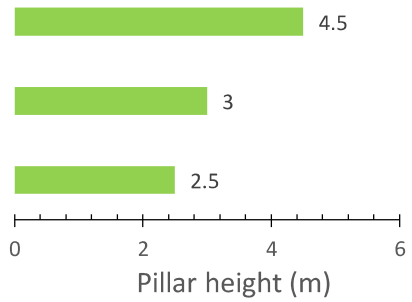

(iv)

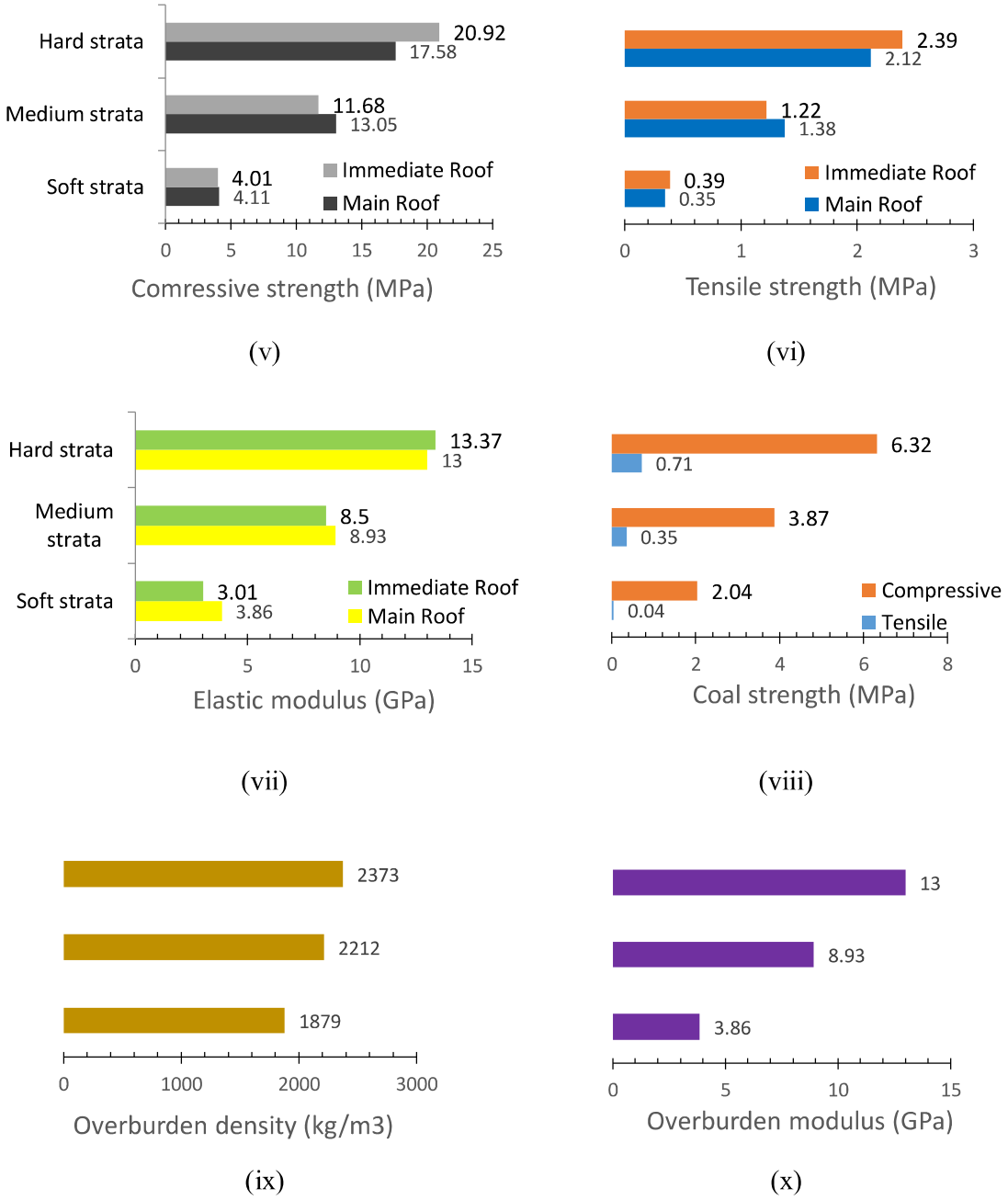

Figure 8.1 Parametric study variables and their range: (i) cover depth, (ii) pillar width, (iii) face length, (iv) pillar height, (v) compressive and (vi) tensile strength of the Caved zone strata, (vii) elastic modulus of the Caved zone strata, (viii) compressive and tensile strength of the coal seam, and (ix) density and (x) elastic modulus of the overburden strata

The floor and overburden strata were assigned the same material properties as the main roof. A total of 1296 experimental models were run for single and double row configurations by considering possible combinations of the parameters.

8.2 Development of Predictive Model for Factor of Safety

The outcomes of all the numerical models for single and double-row chain pillars are presented in Table AVI.1 and Table AVI.2 (Appendix VI), respectively. These outcomes were used to develop predictive models to estimate the FoS of the chain pillar for the single and double-row chain pillar configurations for the given set of parameters in similar conditions.

There are several methods available for developing the predictive model. The conventional methods of regression, such as multiple linear regression (MLR), are based on the process of least squares. Although these methods have been widely used to develop the model in simple cases, they are not suited for problems involving numerous explanatory variables having a complex non-linear relationship with the response variable (Niu et al., 2019). The estimates of the linear regression method get considerably influenced by the existence of even one data set that departs from the general trend (Obi et al., 2020).

In such conditions, artificial intelligence-based methods, which can be trained in different ways, can be used. The most widely used statistical and machine learning methods are kernel methods like the Support Vector Machine (SVM) and the Neural Network (Russell and Norvig, 2016). In this work, the Support Vector Regression (SVR) was used to develop the predictive model of the Factor of Safety of the chain pillar. SVR works on principles similar to Support Vector Machine (SVM). The SVR model does not depend on distributions of the underlying explanatory and response variables; rather, it depends on kernel functions. It helps in better interpretation of the regression model by allowing the construction of a non-linear model without changing the independent variables. The model is constructed using linear, polynomial,

and radial kernel functions which transforms a non-linear problem into a linear problem to obtain the fit in higher-dimension feature space. Vapnik's ε-insensitive loss function, which is analogous to margin in the target values space, is used to extend the SVM to regression estimation (Mercer, 1909) (Figure 8.2).

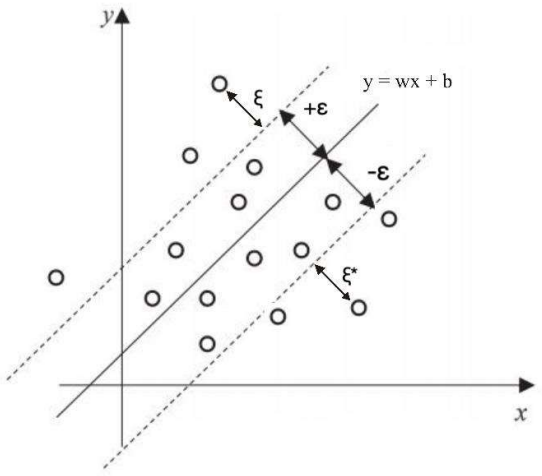

Figure 8.2 Defined hyperplane with an ε tolerance of error and slack variables

The fundamental algorithm behind SVR involves mapping input data (x) into high-dimensional feature space by utilizing a non-linear mapping function $\phi(x)$ and finding a hyperplane $(f(x) = w.\phi(x) + b)$ to separate the target values. The hyperplane is defined by minimizing the following relation (Equation 8.1):

$$E(w) = C\frac{1}{N}\sum_{i=1}^{N}|y_i - f(x_i, w)|_\varepsilon + \frac{1}{2}\|w\|^2 \tag{8.1}$$

where x_i and y_i are the input and the prediction values. $C\frac{1}{N}\sum_{i=1}^{N}|y_i - f(x_i, w)|_\varepsilon$ represents the empirical risk (error) and can be evaluated by ε (Equation 8.2), $\frac{1}{2}\|w\|^2$ is the regularization

term, a measure of the fitness of the function, and C is the regularization constant, which determines the trade-off between the regularization term and the empirical risk.

$$|x|_{\varepsilon} := \begin{cases} 0 & if\ |x| < \varepsilon \\ |x| - \varepsilon & \text{otherwise} \end{cases} \tag{8.2}$$

Equation 8.1 is transformed into an optimal function (Equation 8.3) by introducing positive slack variables ξ_i and ξ_i^* to define the hyperplane by estimating w and b. Slack variables are introduced for the values outside the bound defined by ε.

$$E(w) = C\frac{1}{N}\sum_{i=1}^{N}(\xi_i + \xi_i^*) + \frac{1}{2}\|w\|^2 \tag{8.3}$$

subjected to the following conditions

$$\begin{cases} y_i - f(x_i, w) \leq \varepsilon + \xi_i \\ f(x_i, w) - y_i \leq \varepsilon + \xi_i^* \\ \xi_i, \xi_i^* \geq 0 \end{cases} \tag{8.4}$$

Equations 8.3-8.4 can be transformed into the form as given in Equations 8.5-8.6 as per Karush-Kuhn-Tucker conditions by introducing Lagrange multipliers.

$$L_p(\alpha^*, \alpha) = \varepsilon\sum_{i=1}^{n}(\alpha_i^* + \alpha_i) + \sum_{i=1}^{l} y_i(\alpha_i^* + \alpha_i) + \frac{1}{2}\sum_{i=1}^{N}\sum_{j=1}^{N}(\alpha_i^* + \alpha_i)\left(\alpha_j^* + \alpha_i\right)K\left(x_i, x_j\right) \tag{8.5}$$

subjected to the following conditions:

$$\begin{cases} \sum_{i=1}^{N}(\alpha_i^* + \alpha_i) = 0 \\ \alpha_i^* \geq 0 \\ \alpha_i \leq C \end{cases} \tag{8.6}$$

where $i = 1,2, \ldots, N$, α_i, and α_i^* are Lagrange multipliers. Eventually, the model output is given by the following expression (Equation 8.7):

$$f(x,\alpha) = \sum_{i=1}^{n} (\alpha_i^* + \alpha_i) K(x_i, x_j) + b \tag{8.7}$$

where K (x_i, x_j) is the kernel function which transforms a non-linear problem into a linear problem in higher-dimension feature space to find a fit. Gaussian radial basis function (RBF) kernel is one of the most popular and widely used kernel functions, defined as follows:

$$\mathrm{K}\left(x_i, x_j\right) = \exp\left(-\gamma \left\| x_i, x_j \right\|^2\right) \tag{8.8}$$

where, the parameter γ defines the width of the Gaussian.

The dataset generated from the parametric study was split into two sets: 70% of the data was considered for training the model, while the remaining 30% of the data was considered for testing the model. Before performing regression using the SVR algorithm, the feature scaling was applied using Equation 8.9 to standardize the range of data features so that all the features and explanatory variables are in the same range.

$$\mathrm{x}_{\mathrm{scaled}} = \frac{\mathrm{x} - \mathrm{x}_{\mathrm{min}}}{\mathrm{x}_{\mathrm{max}} - \mathrm{x}_{\mathrm{min}}} \tag{8.9}$$

It is difficult to determine the regularization parameter, C and ε of the SVR model. A rational selection of these parameters is required for a robust model and to avoid overfitting. The risk of overfitting can arise when the value of ε is selected in a small range or C is selected in a large range. Hence, the fitness performance of training data and validation of testing data were considered for different values of these parameters. Consequently, the values of ε and C were determined as 0.001 and 85, respectively, for both the single-row and the double-row configurations of the chain pillars.

8.2.1 Model for Single-Row Chain Pillars

Figure 8.3 shows the fitness performance of the SVR model for the single-row configuration of the chain pillars at the training stage and the cross-validation of the testing data. Figure 8.3 (a) indicates the actual factor of safety obtained from the parametric study against the factor of safety estimated by the SVR model. The model is well trained as each point has a minimal tolerance around the middle line. The estimation error is also close to zero (Fig. 8.4a), as shown by corresponding residual values. A few aberrations are visible for FoS <0.5. Figure 8.3 (b) depicts the cross-validation of the testing data. The model has a small error in the estimated safety factor at the testing stage, as confirmed by corresponding residual values in Figure 8.4 (b).

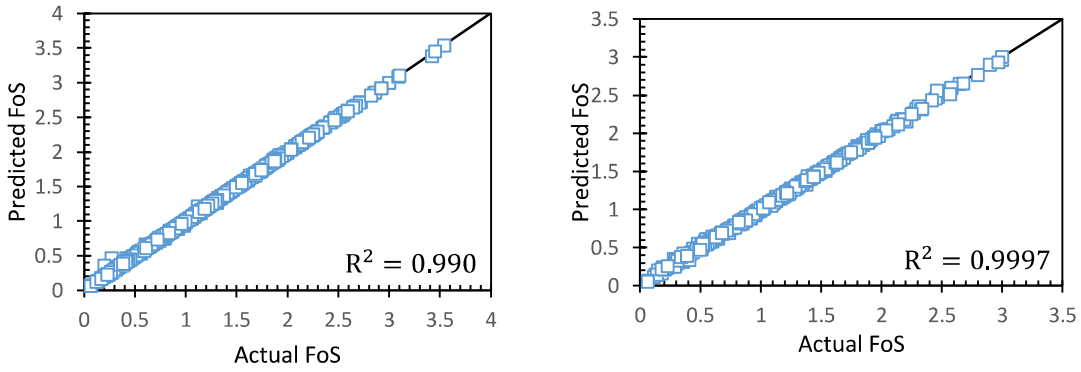

(a) Performance of the SVR model to fit on the training data set

(b) Performance of the SVR model to fit on the testing data set

Figure 8.3 Cross-validation of SVR model for single-row chain pillars; comparison of predicted and actual factor of safety values for (a) training set and (b) testing set

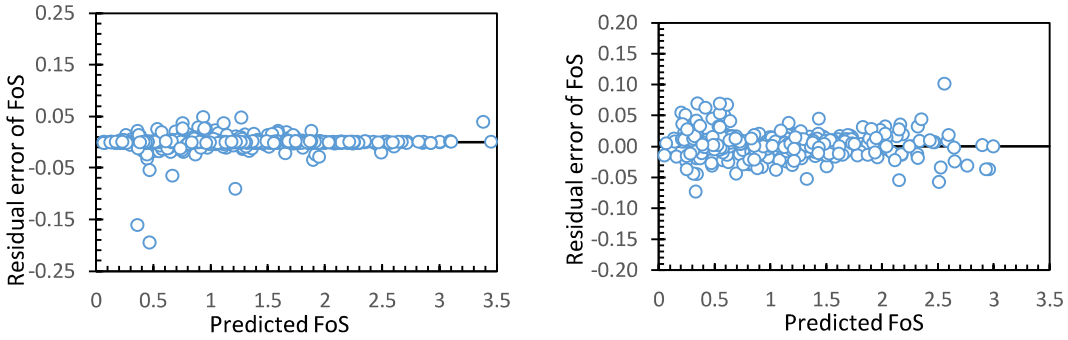

(a) Variation of residual values predicted for training data set

(b) Variation of residual values predicted for testing data set

Figure 8.4 Variation of residual error values as predicted by SVR model for the single-row configuration of chain pillars

8.2.2 Model for Double Row Chain Pillars

Figure 8.5 shows the fitness performance of the SVR model during the training and the cross-validation stages of the testing data for the double-row configuration of chain pillars. Figure 8.5 (a) indicates the actual factor of safety obtained from the numerical modelling study against the SVR model estimated factor of safety. The model is well trained at each point, as indicated by a minimal tolerance around the middle line. The estimation error is also close to zero (Figure 8.6a). Figure 8.5b depicts the cross-validation of the testing data. The model has a small error in the estimated safety factor at the testing stage, as confirmed by the plot of residual values (Figure 8.6b).

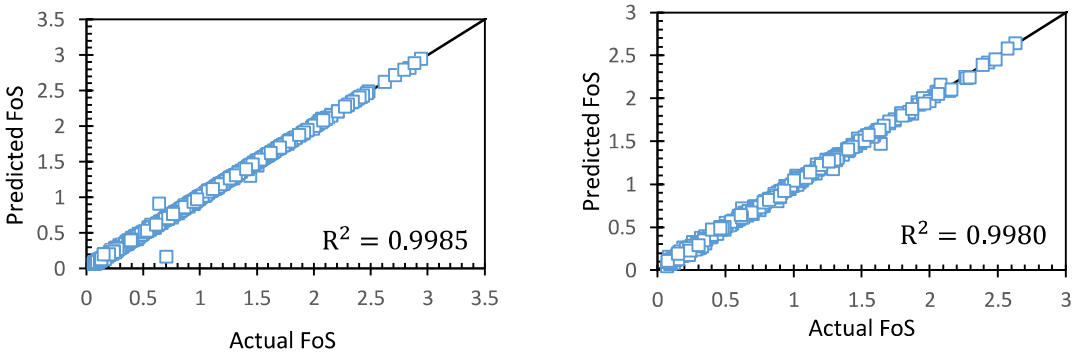

(a) Performance of the SVR model to fit on the training data set

(b) Performance of the SVR model to fit on the testing data set

Figure 8.5 Cross-validation of SVR model for double row chain pillars; comparison of predicted and actual factor of safety values for (a) training set and (b) testing set

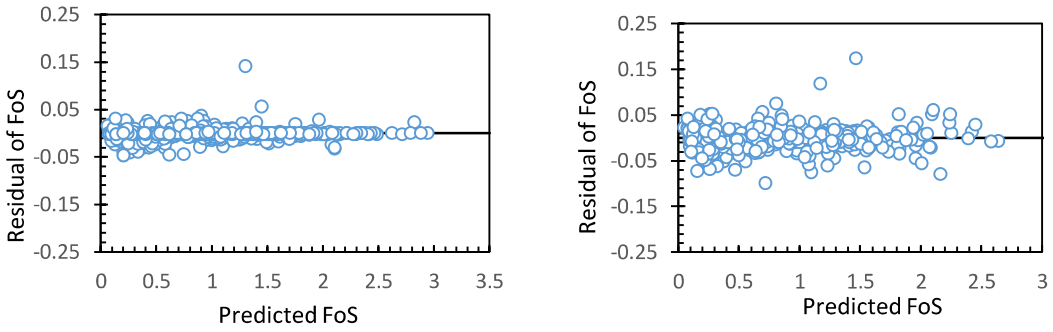

(a) Variation of residual values predicted for training data set

(b) Variation of residual values predicted for testing data set

Figure 8.6 Variation of residual error values as predicted by SVR model for the double-row configuration of chain pillars

8.3 Performance Evaluation of the Model

Figure 8.3 showed that the model could explain 99.97 % of the variance in training data and 99.90% of the variance in the testing data of single-row chain pillars. For double row configuration, the model can explain 99.85% of the variance in the training data and 99.80% variance in the testing data (Figure 8.5).

The fitness performance of the SVR models has been further established using Variance Account For (VAF), Mean Absolute Percentage Error (MAPE), and Root Mean Square Error (RMSE), as given below:

$$\mathrm{VAF} = \left[1 - \frac{\mathrm{var}(\mathrm{y} - \hat{\mathrm{y}})}{\mathrm{var}(\mathrm{y})}\right] \times 100 \tag{8.10}$$

$$\mathrm{RMSE} = \sqrt{\frac{1}{N}\sum_{i=1}^{N}(\mathrm{y}_i - \hat{\mathrm{y}}_i)^2} \tag{8.11}$$

$$\mathrm{MAPE} = \frac{1}{N}\sum_{i=1}^{N}\left|\frac{\mathrm{y}_i - \hat{\mathrm{y}}_i}{\mathrm{y}_i}\right| \times 100 \tag{8.12}$$

where y and $\hat{\mathrm{y}}$ are observed and predicted values.

Table 8.2 R^2, RMSE, VAF, and MAPE of the SVR model for training and testing data sets of single and double-row chain pillars

Chain pillar configuration	Data set	R^2 (Ideal value = 1)	RMSE (Ideal value = 0)	VAF (Ideal value =100)	MAPE (Ideal value = 0)
Single row	Training	0.9997	0.011134	99.97	0.5511
	Testing	0.9990	0.019160	99.90	2.1326
Double row	Training	0.9985	0.022083	99.85	0.0114
	Testing	0.9980	0.025510	99.80	0.0441

The statistical indicators in Table 8.2 confirm the higher accuracy of the SVR model for predicting the factor of safety of the single and the double row chain pillars for a set of independent variables considered in this study.

8.4 Influence of Critical Parameters on the Stability of Chain Pillars

The machine learning (ML) model as developed above was used to quantify the influence of critical parameters on the stability of the chain pillar. Table 8.3 shows the base value of the input parameters, their range and the interval of variation.

Table 8.3 Basic value of the critical parameters and their range of variation and interval for single and double–row chain pillars

Parameters	Basic value		Variation range (Interval)	
	Single row	Double row	Single row	Double row
Pillar width (m)	48	15	25-95 (10)	10-45 (10.0)
Pillar height (m)	3.0		2.5 - 4.5 (0.5)	
Cover depth (m)	500		350 - 850 (100)	
Coal strength (MPa)	6.32		2.04 - 6.32 (1.0)	
Abutment angle (°)	30.4		0 - 80 (10.0)	
Face length (m)	200		150 - 250 (20)	
Caving height (m)	45		37.5 - 67.5 (7.5)	
Overburden density (kg/m^3)	2345		2000 - 2345 (100)	
Overburden modulus (GPa)	13.0		4 - 12 (2.0)	
Modulus ratio	43.45		2.90-43.45 (20.0)	

Figure 8.7 shows the variation in the factor of safety of the single and double-row chain pillars with the change in the control variables. The pillar's safety factor increases monotonically with an increase in pillar width, coal strength, abutment angle, moduli ratio between pillar and roof, and pillar and floor. It decreases with an increase in pillar height, cover depth, face length, caving height, overburden density and modulus.

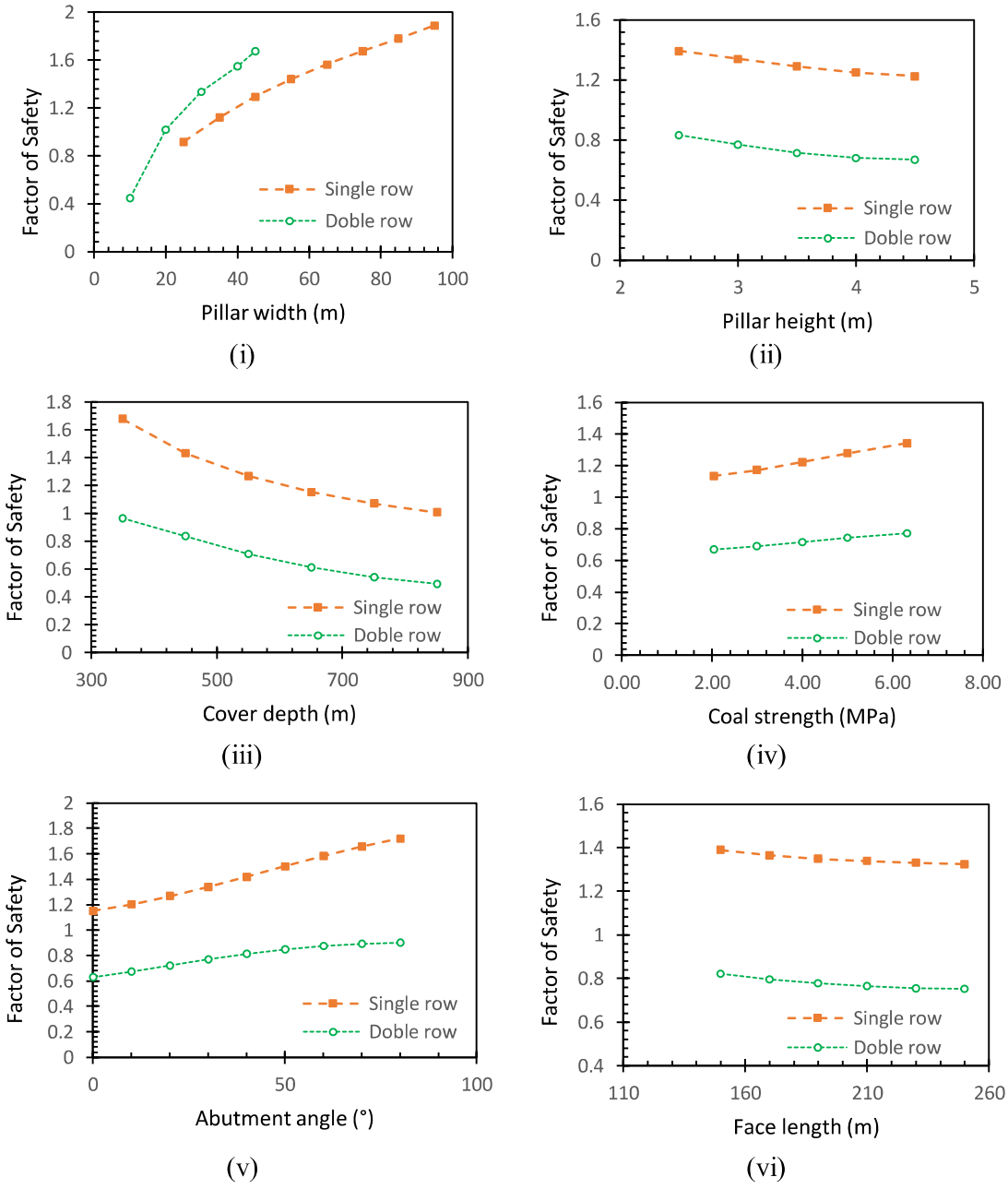

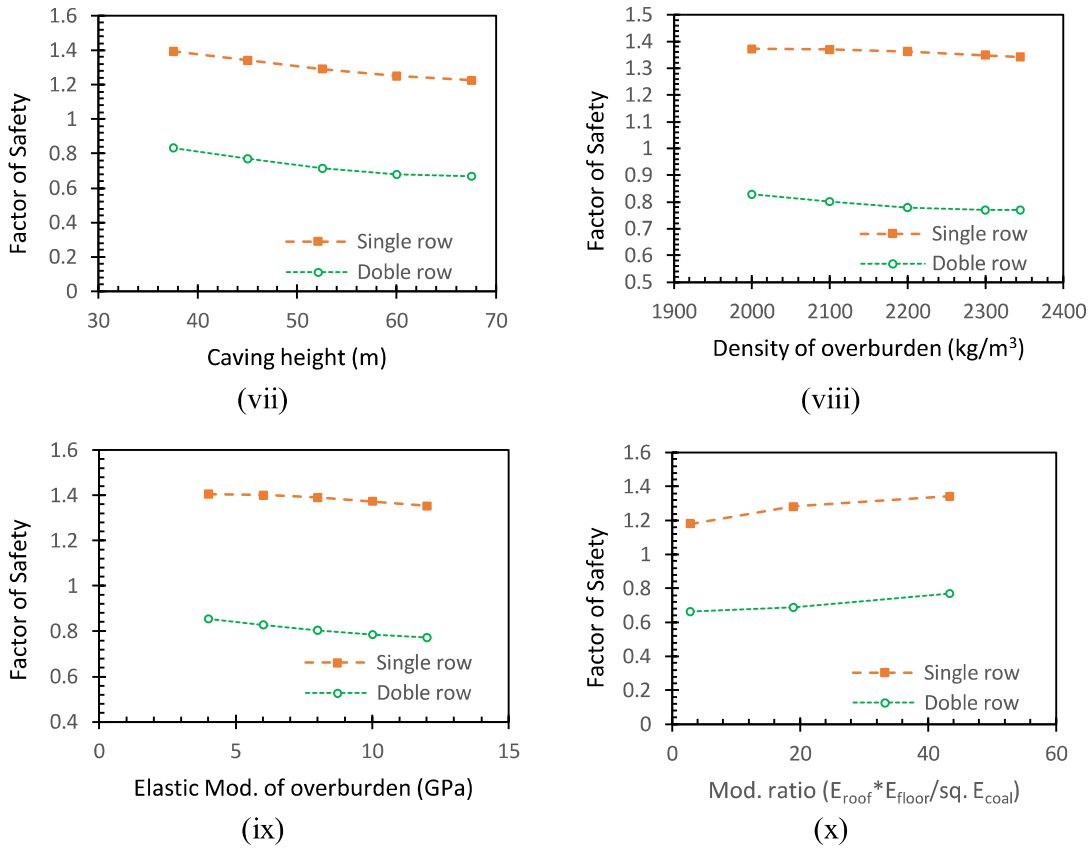

Figure 8.7 Variation in the factor of safety of the single and double row chain pillars with the change in the value of the parameter: (i) pillar width, (ii) pillar height, (iii) cover depth, (iv) coal strength, (v) abutment angle, (vi) face length, (vii) caving height, (viii) density and (ix) elastic modulus of the overburden strata, and (x) ratio of the roof and floor modulus to the coal seam modulus.

These observations agree with the findings of several previous works (Choi and McCain, 1980; Hsuing and Peng, 1985; Mark and Bieniawski, 1986; Chokhani, 2012; Rezaei et al., 2015a; Colwell, 1998; Frith and Reed, 2019). However, these works attempted to separately estimate the abutment load and the pillar strength. Hence, they could only quantify the loading aspect of the abutment angle, concluding that the factor of safety of the pillar decreases with an increase in abutment angle. On the other hand, the factor of safety estimated using the integrated approach considers the loading and confining aspects of the abutment angle, concluding that the FoS of the pillar increases with an increase in the abutment angle. This observation shows good agreement with the findings reported by Chokhani (2012).

8.5 Summary

A numerical modelling exercise was carried out to evaluate the effect of several geo-mining parameters on the chain pillar stability when both the adjoining panels had been mined out. The pillar stability was assessed in terms of the factor of safety. A comprehensive study involving 1296 data sets for single row and double row chain pillar configurations was carried out using two-dimensional plain-strain numerical modelling for the variation in pillar height from 2.5 - 4.5 m, cover depth from 350 - 900 m, face length from 150 – 250 m with soft, medium, and hard strata and coal seams. While the caving height was taken as 15 times the extraction height, the pillar width varied from 25 – 100m and 10 – 47.5 m for single row and double row configurations, respectively.

The outcomes of the 1296 experimental models for each of the single row and double row configurations were utilized to develop Machine Learning (ML) based regression models. 70% of the dataset was used for training, while 30% was used for testing. The performance of ML models was evaluated in terms of fit to the training and testing sets along with some popular indicators such as variance account for (VAF), mean absolute percentage error (MAPE), and root mean square error (RMSE). The performance evaluation showed that the models were well trained and could predict the factor of safety with reasonable accuracy.

The ML models for single row and double row configurations were used to study the influence of several considered parameters on the factor of safety of the typical pillar case. It was observed that the safety factor increased monotonically with an increase in pillar width, coal strength, abutment angle, and moduli ratio between pillar and roof and pillar and floor. The FoS decreased with increased pillar height, cover depth, face length, caving height, overburden density and modulus. These observations are in good agreement with the findings of other researchers from across the world (Choi and McCain, 1980; Hsuing and Peng, 1985; Mark and Bieniawski, 1986; Chokhani, 2012; Rezaei et al., 2015; Colwell, 1998; Frith and Reed, 2018).